THE JOURNAL OF PHYSICAL CHEMISTRY LETTERS
A JOURNAL OF THE AMERICAN CHEMICAL SOCIETY

pubs.acs.org/JPCL

Letter

Energy-Conserving and Thermally Corrected Neglect of Back-Reaction Approximation Method for Nonadiabatic Molecular Dynamics

Alexey V. Akimov*

Cite This: J. Phys. Chem. Lett. 2023, 14, 11673−11683

Read Online

ACCESS | Metrics & More | Article Recommendations | Supporting Information

ABSTRACT: In this work, the energy-conserving and thermally corrected neglect of the back-reaction approximation approach for nonadiabatic molecular dynamics in extended atomistic systems is developed. The new approach introduces three key corrections to the original method: (1) it enforces the total energy conservation, (2) it introduces an explicit coupling of the system to its environment, and (3) it introduces a renormalization of nonadiabatic couplings to account for a difference between the instantaneous nuclear kinetic energy and the kinetic energy of guiding trajectories. In the new approach, an auxiliary kinetic energy variable is introduced as an independent dynamical variable. The new approach produces nonzero equilibrium populations, whereas the original neglect of the back-reaction approximation method does not. It yields population relaxation time scales that are favorably comparable to the reference values, and it introduces an explicit and controllable way of dissipating energy into a bath without an assumption of the bath being at equilibrium.

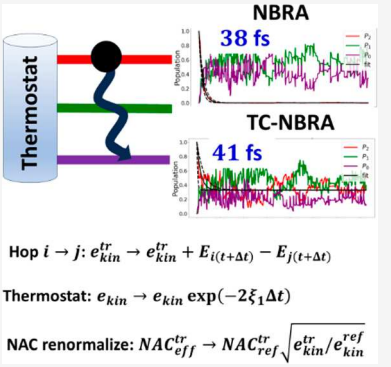

Nonadiabatic molecular dynamics (NA-MD) is a widely adopted family of computational methods to model quantum dynamics of excited states in various systems.[1−5] The NA-MD simulations have found their use in describing various kinds of processes in many molecular and condensed-matter systems: modeling nonradiative electron−hole recombination and "hot" carrier relaxation in quantum dots and molecular clusters,[6−13] nanotubes,[14,15] plasmonic systems,[16] or exotic states of matter;[17] modeling photoinduced isomerization and reactive processes in various molecular systems;[18−22] and modeling charge transfer and charge carrier trapping processes in 2D materials,[23−31] interfaces,[25,32−36,36,37] organic solids,[38,39] and pristine and defect-containing bulk semiconductors.[40−46]

Computing the nonadiabatic dynamics in atomistic and solid-state systems has been made possible by adopting quantum-classical trajectory surface hopping (TSH) techniques,[4,47−51] among which Tully's fewest switches surface hopping (FSSH)[52] has been one of the most popular choices due to its simplicity to implement and clear physical picture. Together with the FSSH, a number of other TSH schemes have been in use, aiming to address known deficiencies of the FSSH, such as its over-coherence[53−69] or its reliance on the ill-behaved nonadiabatic couplings (NACs).[50,70−73] Such methods replace the fully quantum mechanical treatment of nuclear evolution with a classical evolution while keeping the description of electronic degrees of freedom quantal. To account for quantum-mechanical branching, nuclear wavepackets are mimicked by swarms of classical or semiclassical trajectories, coupled or uncoupled to each other, evolving on the individual or effective potential energy surfaces (PES). In this way, nuclear evolution is sensitive to changes of electronic states, and the electronic evolution is affected by the histories of nuclear trajectories. This is the situation of a self-consistency of electronic and nuclear degrees of freedom (DOF), also termed the electron−nuclear back-reaction. In the following discussion, such a self-consistency is referred to as the non-neglect of back-reaction approximation (non-NBRA) to juxtapose it with the neglect of back-reaction approximation (NBRA) strategy introduced below.

Extending the TSH simulations to systems with hundreds and thousands of atoms requires another widely used approximation, the NBRA, pioneered by Prezhdo and co-workers,[74−76] although new methodological developments facilitate the readoption of the non-NBRA approaches with correct back-reaction to model NA-MD in large systems.[77−83] Within the NBRA, changing the active electronic state (e.g., during stochastic hop) is assumed to not affect the nuclear dynamics; no velocity rescaling as in FSSH is conducted, and the future evolution of nuclei remains unchanged. Thus, the NBRA enables using a limited number of precomputed nuclear trajectories (in practice, just one is often used) in computations of electronic dynamics. However, electronic dynamics does not

Received: October 29, 2023
Revised: November 26, 2023
Accepted: December 13, 2023
Published: December 18, 2023

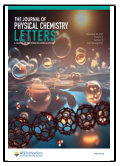

https://doi.org/10.1021/acs.jpclett.3c03029
J. Phys. Chem. Lett. 2023, 14, 11673−11683

exert any back-reaction on nuclei and hence does not generate multiple histories of nuclear evolution, justifying the use of a small number of precomputed trajectories. Thus, the use of NBRA is often considered appropriate if no significant nuclear rearrangement (e.g., isomerization, bond breaking, etc.) is expected to occur in the studied process, which is often the case for "rigid" molecules or clusters, nanoscale systems, and periodic solids.

In the regular (non-NBRA) TSH methods, the possibility of electronic transitions to higher energy states is determined based on the possibility of conserving the total energy. This energy conservation principle is used to define frustrated (unallowed) hops to higher energy states. Since nuclear velocities are not rescaled in the NBRA framework, the proposed stochastic hops to upper energy states are accepted with the Boltzmann probability, $\exp(-\Delta E_{ij}/k_B T)$, while the total energy is not conserved. One can regard the NBRA procedure as dissipative dynamics with an implicit bath. The Boltzmann factor is, however, a signature of an equilibrium environment. Thus, the NBRA approach implicitly relies on the assumption of the system being in thermal equilibrium with the equilibrated environment, which is a better-justified assumption for intrinsically slow nonadiabatic processes, such as electron−hole recombination, than for ultrafast processes, such as "hot" carrier cooling.

Furthermore, the TSH procedure in the NBRA simulation relies on nonadiabatic couplings (NACs) or, equivalently, time-overlaps computed for trajectories sampled by a ground-state molecular dynamics (MD) procedure. Because there is no velocity rescaling in the NBRA calculations, NACs remain insensitive to the instantaneous nuclear momenta. This is unlike the explicit TSH procedure, where NACs are computed as $d_{ij} = \sum_\alpha \left\langle \psi_i | d/dR_\alpha | \psi_j \right\rangle P_\alpha / M_\alpha$ and hence explicitly depend on nuclear momenta, or, equivalently, on instantaneous nuclear kinetic energy. Combined with the idea of velocity rescaling, this momentum sensitivity of NACs leads to a qualitative difference in modeling of electronic transition processes within NBRA and non-NBRA approaches. Within the NBRA, the transition from a higher energy state to the lower energy state would not affect the probability of the reverse transition, since both would be proportional to the same NAC magnitude. In fact, the reverse transition would be strongly inhibited by the Boltzmann factor. In contrast, in the non-NBRA treatment, the transition from the upper state to the lower state would increase the effective NAC for the reverse transition due to increased momenta after rescaling, at least before such kinetic energy excess is distributed across other nuclear vibrations. Moreover, the inverse transition is not inhibited by any artificial factors as long as the nuclear subsystem has sufficient kinetic energy in the direction of the corresponding nonadiabatic derivative coupling vector. In the isolated system, population oscillations would be common (e.g., Rabi oscillation as a limiting case). Population relaxation would be possible only by removing kinetic energy from such modes, which can be realized via intra- or intermolecular vibrational energy transfer. This aspect of energy removal as well as the asymmetry of effective NACs for the up-to-down vs down-to-up energy transition are fully ignored by the phenomenological NBRA approach.

In this work, I revise the NBRA methodology to introduce total energy conservation and account for the two missing effects discussed above. First, the resulting method introduces auxiliary kinetic energy variables that are evolved to maintain the total energy balance. Similar to the original NBRA approach, no explicit treatment of nuclear momenta is needed. The auxiliary variables are used to introduce thermal correction to effective NACs to account for the difference of the system's effective kinetic energy in its lower vs higher electronic energy states. When using such auxiliary variables, hops to higher energy states are proposed and accepted more frequently than in standard NBRA. Second, the new approach introduces an explicit kinetic energy dissipation mechanism by coupling the introduced auxiliary kinetic energy variables to an effective thermostat with controllable parameters. The thermostated auxiliary energy variables account for phenomenological intra- and intermolecular vibrational energy transfer. Unlike the Boltzmann factor-based NBRA approach, the rates of such vibrational energy transfer are the controlled parameters of the simulation and can be chosen to represent a nonequilibrium environment.

In this work, Tully's FSSH method is chosen to model NA-MD. The shortcomings of the method regarding its over-coherence are well-known.[67] However, since the focus of the present work is on a different aspect of the NA-MD methodology, the choice of the simplest FSSH approach is suitable. The key equations of the generic FSSH framework and its NBRA variant are detailed in the Supporting Information. To summarize, in both variants the electronic degrees of freedom are described by quantum mechanical time-dependent Schrodinger equation (TD-SE), while the nuclei are treated classically. In the non-NBRA variant, the evolution of the nuclei is governed by the forces corresponding to the active adiabatic state, while the NBRA variant uses the precomputed trajectories. The nuclear momenta are rescaled or reversed in the non-NBRA calculations, depending on the possibility of electronic transitions, while in the NBRA-FSSH no explicit nuclear momenta are used, so no momenta rescaling or reversal is conducted. The nuclear trajectories used in NBRA are obtained by integrating eq S6 in some way, such as using an adiabatic MD on the ground state or even using trajectories obtained from the non-NBRA simulations. Such precomputed trajectories are convenient to call the guiding trajectories because they define the sequence of time-dependent vibrational Hamiltonians, eq S4, and hence guide the evolution of electronic variables and the subsequent stochastic surface hop events.

In the present work, the guiding trajectories are taken as the non-NBRA FSSH trajectories. The vibronic Hamiltonians, NACs and time-overlaps computed along such trajectories are used to integrate eq S3 and to compute hop proposal and acceptance probabilities in the NBRA. Such an approach facilitates the comparison of the results of the NBRA and non-NBRA calculations. All the methods reported in this work are implemented in the Libra package,[84,85] version 5.5.0. This package is also used to conduct all of the calculations presented in this work.

It is now time to introduce the new approach, dubbed thermally corrected NBRA (TC-NBRA). Generally, it follows the recipe of NBRA but introduces three main modifications.

(1) The time-local conservation of the total energy is introduced during the adiabatic evolution and at the nonadiabatic transitions.

$$E^{\mathrm{tr}}_{\mathrm{tot}}(t) = E^{\mathrm{tr}}_{i(t)}(t) + e^{\mathrm{tr}}_{\mathrm{kin}}(t) = \mathrm{const} \quad (1)$$

Here, $e^{\mathrm{tr}}_{\mathrm{kin}}(t)$ is the instantaneous kinetic energy of a trajectory "tr". It is regarded an auxiliary dynamical variable. Here $E^{\mathrm{tr}}_{i(t)}$ denotes the adiabatic energy of the

https://doi.org/10.1021/acs.jpclett.3c03029
J. Phys. Chem. Lett. 2023, 14, 11673−11683

active adiabatic state i, which can change in time, $i = i(t)$, because of stochastic hops. The variable $e_{\mathrm{kin}}^{\mathrm{tr}}$ is used instead of explicitly considering nuclear momenta for all the trajectories.

Equation 1 is used in two ways. First, we note that, because of the underlying NBRA, there is no change of nuclear momenta in response to changing the nuclear geometry of the system when evolving adiabatically from time t to time $t + \Delta t$, $\boldsymbol{R}(t) \rightarrow \boldsymbol{R}(t + \Delta t)$. To reflect such a change, the kinetic energy variable, $e_{\mathrm{kin}}^{\mathrm{tr}}$, is evolved to enforce the total energy conservation, but only locally, as a component of the overall update recipe for this variable at each time interval: $e_{\mathrm{kin}}^{\mathrm{tr}}(t) \rightarrow e_{\mathrm{kin}}^{\mathrm{tr}}(t + \Delta t) = e_{\mathrm{kin}}^{\mathrm{tr}}(t) + E_{i(t)} - E_{i(t+\Delta t)}$. Such an update is done after each evaluation of the Hamiltonian. Also note that $i(t + \Delta t)$ can change compared to $i(t)$ adiabatically as a result of the trivial crossing resolution. This resolution is done based on the local diabatization reprojection matrix as detailed elsewhere.[50]

Second, the kinetic energy variable $e_{\mathrm{kin}}^{\mathrm{tr}}$ is used to determine the conditions of the proposed hop acceptance: $P_{tr,i\rightarrow j}^{acc,TC\text{-}NBRA\text{-}FSSH}(t,t + \Delta t) = \Theta(E_{i(t+\Delta t)}^{\mathrm{tr}}(t + \Delta t) + e_{\mathrm{kin}}^{\mathrm{tr}}(t + \Delta t) - e_{j(t+\Delta t)}^{\mathrm{tr}})$, with the abbreviations and symbols defined in section S1 of the Supporting Information. If the proposed hop is accepted, the kinetic energy variable is updated to reflect the total energy conservation in the nonadiabatic transition, $e_{\mathrm{kin}}^{\mathrm{tr}}(t + \Delta t) \rightarrow e_{\mathrm{kin}}^{\mathrm{tr}}(t + \Delta t) + E_{i(t+\Delta t)} - E_{j(t+\Delta t)}$. As before, the total energy conservation is enforced locally, only as an update to this part of the TC-NBRA computational workflow. In the present approach, the kinetic energy variable can be regarded as a proxy to nuclear momenta, which are not used directly within the NBRA framework. In the non-NBRA simulations, the momenta can be updated in the direction of adiabatic forces during the adiabatic evolution. During the nonadiabatic transitions, the momenta can be updated in the direction parallel to derivative coupling vectors, momenta, of force gradients. However, the present approach is formulated to not need any of this information (the premises of the NBRA framework). Even more importantly, in the NBRA framework, one should work within the precomputed guiding trajectories and is not allowed to modify them. The use of the auxiliary kinetic energy variables allows all these restrictions to be addressed, enforcing energy conservation principle and determining the hop acceptance probabilities in an aggregate way without knowledge of neither the atomically resolved momenta nor additional properties such as derivative coupling vectors.

(2) The kinetic energy variables introduced above, $e_{\mathrm{kin}}^{\mathrm{tr}}$, are coupled to a thermostat. Because of this coupling the total energy of the system, $E_i^{\mathrm{tr}} + e_{\mathrm{kin}}^{\mathrm{tr}}$, does not need to be conserved. In the present work, the Nosé−Hoover chain (NHC) thermostat is used.[86] When applied to classical nuclei, it changes the nuclear EOM, eq S6b, by introducing a friction term:

$$\dot{\boldsymbol{P}}(t) = \boldsymbol{F}_i - \xi_1 \boldsymbol{P}(\mathrm{t}) \tag{2}$$

where ξ is the velocity of the thermostat immediately coupled to the system (the one with the index 1, hence ξ_1). The effect of the thermostat variables ξ_1 is to rescale the momenta by an exponential factor: $\boldsymbol{P}(t) \rightarrow \boldsymbol{P}(t + \Delta t) = \boldsymbol{P}(t)\ \exp\ (-\xi_1 \Delta t)$. However, such a use of the NHC thermostat would require knowing the momenta. One can observe that since all momenta are rescaled uniformly, one can apply the effect of the thermostat directly to the auxiliary kinetic energy variable: $e_{\mathrm{kin}}(t) \rightarrow e_{\mathrm{kin}}(t + \Delta t) = e_{\mathrm{kin}}(t)\exp\ (-2\xi_1 \Delta t)$. The NHC variables evolve as summarized in section S2 of the Supporting Information. Analysis of such equations shows that solving this equation requires only the instantaneous nuclear kinetic energy and not the individually resolved nuclear momenta. Thus, the use of the auxiliary kinetic energy variable is sufficient and leads to a consistent set of equations. To reiterate, this variable evolves due to both the adiabatic and nonadiabatic transitions, and is modified due to coupling to the effective thermostat.

While the total energy of system, $e_{\mathrm{kin}} + E_i$, can fluctuate or decay, the total extended energy $e_{\mathrm{kin}} + E_i + E_{\mathrm{therm}}$ that includes the energy of thermostat, E_{therm}, as defined in eq S9 is expected to be conserved. Furthermore, for very low thermostat frequencies, $\nu \rightarrow 0$, the effect of the thermostat vanishes, and one can expect the system's energy, $e_{\mathrm{kin}} + E_i$, to be conserved. Such an energy conservation condition is equivalent to the absence of system's energy dissipation to the environment/bath. Under such a condition, higher energy states may be repopulated due to thermally assisted excitations.

(3) Finally, the last ingredient of the TC-NBRA approach is what the TC acronym stands for: the thermal correction of NACs. Indeed, the NACs, eq S5, obtained in an adiabatic ground-state evolution imply that the momenta (and the reference kinetic energy, $e_{\mathrm{kin}}^{\mathrm{ref}}$) correspond to values that naturally develop during such an evolution. In NA-MD simulations, when a nonadiabatic transition from a higher-energy state to a lower-energy state occurs, the instantaneous kinetic energy, $e_{\mathrm{kin}}^{\mathrm{tr}}$, can be large until it is dampened by the thermostat (or by an explicit mechanism of vibrational energy transfer). As a consequence, the effective NACs may become larger than the ones computed at the reference kinetic energy, $e_{\mathrm{kin}}^{\mathrm{ref}}$. Assuming a uniform rescaling of momenta, the amplification factor should be $NAC_{\mathrm{eff}}^{\mathrm{tr}} = NAC_{ref}^{\mathrm{tr}}\sqrt{e_{\mathrm{kin}}^{\mathrm{tr}}/e_{\mathrm{kin}}^{\mathrm{ref}}}$. Alternatively, one can consider transitions to the higher-energy states. In this scenario, the instantaneous kinetic energy, $e_{\mathrm{kin}}^{\mathrm{tr}}$, may become smaller than the reference kinetic energy, $e_{\mathrm{kin}}^{\mathrm{ref}}$. The effective NACs would be downscaled, leading to slower up-energy transitions than expected in regular NBRA simulations.

The presented NAC rescaling approach is based on an implicit assumption of a uniform rescaling of nuclear momenta along the current directions. In principle, the momenta could be rescaled in different directions (e.g., along the derivative coupling vectors). However, as noted above, the TC-NBRA method is formulated to be applicable within a typical NBRA workflow, where the NAC vectors are usually not available. Furthermore, as the recent work of Barbatti[87] demonstrates, the uniform velocity rescaling may perform well compared to the desired velocity rescaling along the derivative coupling vectors. Alternative, refined NAC scaling approaches should be possible within the TC-NBRA method depending on the availability of additional information, such as energy gradients or derivative coupling vectors.

https://doi.org/10.1021/acs.jpclett.3c03029
J. Phys. Chem. Lett. 2023, 14, 11673−11683

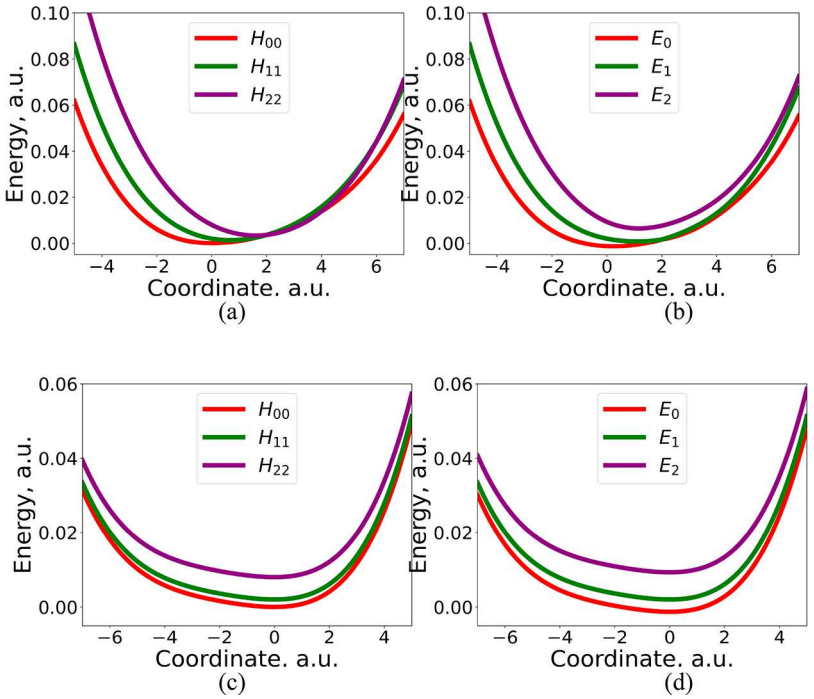

Figure 1. Potential energy profiles of the Tully−Parandekar Hamiltonian, eq 3a, along each of the two coordinates: (a and b) quantum coordinate q_0 and (c and d) bath coordinate q_1. (a and c) Diabatic surfaces. (b and d) Adiabatic surfaces. All PES profiles are computed with a nonscan coordinate fixed at a value of 0.0.

Finally, a few exceptional situations are worth discussing. First, in TC-NBRA, one needs to specify the initial total energy level. Due to the time-local energy conservation conditions discussed above, the nonadiabatic transitions to the levels with the total energy higher than the one set initially would be impossible, since such transitions would be rejected. Second, the evolution of the kinetic energy variable due to an adiabatic transition can lead to negative kinetic energies. This is a consequence of the intrinsic inconsistency of nuclear momenta and coordinates (momenta are not adjusted to reflect the forces at the guiding trajectories) combined with the kinetic energy dissipation into a thermostat. The inconsistency is lower when the thermostat is absent, but even in this situation negative auxiliary kinetic energy values are still possible. Empirically, it is found that when the kinetic energy variables become negative, it is best not to apply thermostat rescaling to them. Third, the kinetic energy along the guiding trajectory should be computed (which is usually not a problem in atomistic simulations) for TC-NBRA calculations. This property is used as $\epsilon_{\text{kin}}^{\text{ref}}$. In situations in which it is numerically zero, no NAC rescaling is conducted to avoid divergences.

The TC-NBRA approach is compared to the regular NBRA method, with the expectation of having comparable dynamics in both cases but also having some differences too. Both TC-NBRA and NBRA methods are also compared to the non-NBRA calculations as well, although to mainly learn the differences; there is no an priori expectation of the NBRA methods to be comparable to the non-NBRA ones.

For demonstration purposes, a model three-level system coupled to a classical anharmonic bath is considered. The Hamiltonian in the diabatic representation is given by

$$H_{ii} = E_i + \frac{1}{2}k_i(q_0 - \overline{q}_i)^2 + \sum_{i=0}^{N-1} V_0(a^2 q_{i,i+1}^2 - a^3 q_{i,i+1}^3 + 0.58a^4 q_{i,i+1}^4) \tag{3a}$$

$$H_{ij} = V_{ij},\ i \neq j \tag{3b}$$

Here, $E_0 = 0$ Ha, $E_1 = 0.001$ Ha, $E_2 = 0.002$ Ha, $\overline{q}_0 = 0.0$ Bohr, $\overline{q}_1 = 1.0$ Bohr, $\overline{q}_2 = 2.0$ Bohr, $k_0 = 0.001$ Ha/Bohr^2, $k_1 = 0.002$ Ha/Bohr^2, $k_2 = 0.003$ Ha/Bohr^2, $V_0 = 0.01$ Ha, $a = 0.25$, $V_{01} = V_{10} = V_{02} = V_{20} = V_{12} = V_{21} = 0.002$ Ha, $q_{i,i+1} = q_i - q_j$, and N is the number of nuclear DOFs. The second term in eq 3a represents the bath modes and is chosen as in prescription of Tully and Parandekar.[88−90] In particular, I consider the simplest case of two nuclear DOFs. Out of these two, the DOF q_0 is regarded as "quantum", that is, NACs are computed with respect to only this variable. In addition, only this DOF is considered in velocity rescaling after accepted hops, and only this DOF is used to determine whether the proposed hop is allowed in the non-NBRA calculations. For these reasons, in the TC-NBRA, there number of degrees of freedom of the thermostated system is set to 1, $g_f = 1$, eqs S8c, S8e, and S9. The second mode, q_1, is regarded as a classical bath mode. The PES profiles for all energy states along each of the two coordinates (q_0 and q_1) are shown in Figure 1.

In the present work, the guiding trajectories are obtained by the non-NBRA FSSH procedure, with the nuclear DOFS initialized as $q_0 = -4$, $q_1 = 1.0$ au and $p_0 = p_1 = 0$ au The initial adiabatic electronic state is chosen as either 0 (red) or 2 (purple), leading to different nuclear trajectories. The dynamics is integrated for 15 000 time steps, with the integration timesteps for electronic and nuclear DOFs chosen to be 5 au of time. Although it is common to use the adiabatic ground-state dynamics to produce guiding trajectories for subsequent NBRA calculations, in this work, I choose to use the FSSH approach.

https://doi.org/10.1021/acs.jpclett.3c03029
J. Phys. Chem. Lett. 2023, 14, 11673−11683

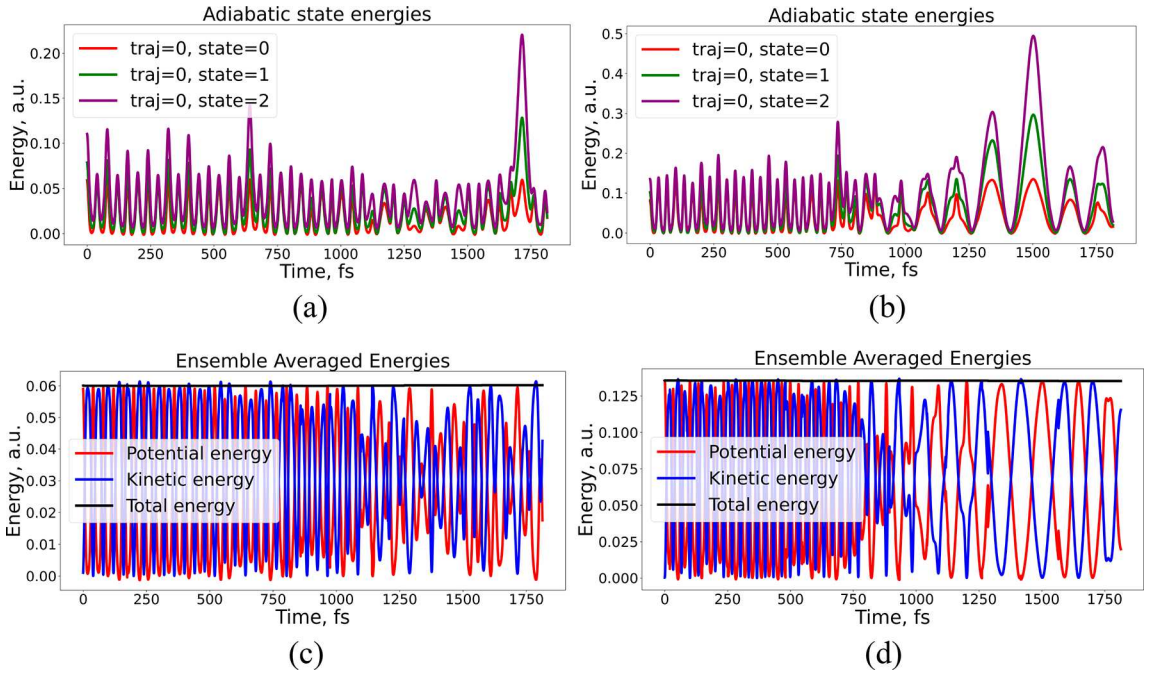

Figure 2. Evolution of (a and b) adiabatic energy level and (c and d) total, kinetic, and potential energies along the two guiding trajectories used. The guiding trajectories are obtained by the FSSH procedure starting in adiabatic (a and c) state 0 or (b and c) state 2 with an initial nuclear coordinate at $q = -4$ au and zero nuclear momentum.

There is no a priori expectation for the NBRA and non-NBRA results to match each other, but using the same nuclear trajectories minimalizes the number of varied parameters and facilitates the comparison of the two methods. One can also consider the FSSH trajectory with the initial electronic state set to 0 as the closest analogue of typical NBRA trajectories (the only difference would be that the nonadiabatic transitions are allowed in the present sampling). The resulting trajectories are used in the NBRA and TC-NBRA calculations. The evolution of the three adiabatic energy levels, as well as evolution of kinetic, potential, and total energies in these two FSSH trajectories, is shown in Figure 2.

In all NBRA and TC-NBRA calculations, $N = 250$ stochastic trajectories are used. The computed TSH populations are obtained as the ratio of trajectories residing in a given state i to the total number of trajectories, $P_i^{\mathrm{TSH}}(t) = N_i(t)/N$. The computed TSH populations are used to obtain the relaxation time scales, τ, (only for state 3 relaxation), by fitting TSH population P_2^{TSH} to the exponential decay function of form $f(t) = A + (1 - A)\exp(-t/\tau)$. This procedure is repeated four times (four batches). The repetition is needed to estimate the confidence intervals for computed relaxation time scales (Figure 3).

The population dynamics obtained in the non-NBRA FSSH calculations is shown in Figure 3a and b. These are the calculations based on calculations of $N = 250$ independent TSH trajectories. For each of them, the initial conditions are sampled from a normal distribution centered on initial values of coordinate ($q_0 = 0$ au or $q_0 = -4$ au) and momentum ($p_0 = 0.0$ au). These results are given solely as a higher-accuracy reference, but it is complicated to compare them to the NBRA or TC-NBRA results, since the latter are based on a single nuclear trajectory. The TC-NBRA and NBRA results reported here represent a single snapshot from more comprehensive sampling. Considering that using a single guiding trajectory in atomistic NBRA simulation is a common practice, I primarily focus on a comparison of the SH population dynamics obtained in NBRA and TC-NBRA calculations (as well as compare them to the SE population dynamics from the single non-NBRA trajectory) for the identical guiding trajectories. In fact, rerunning the TC-NBRA and NBRA calculations with alternative guiding trajectories may result in a different set of time scales. Thus, the absolute values of the time scales for population relaxation may vary from a guiding trajectory to a guiding trajectory, but the comparison of the relative trends should remain valid.

Since in this work I focus on comparing the dynamics along a single guiding trajectory (for each istate), the TD-SE-derived populations, $|C_i|^2$, computed along such trajectories are regarded as local references. Note that for the first trajectory (Figure 3c) the initial population of the ground state is 1, $P_0(t = 0) = 1$, while in the second trajectory (Figure 3d) the initial population is on the third state, $P_2(t = 0) = 1$. In the following NBRA and TC-NBRA tests, all NA-MD simulations start on the third state; therefore, I do not attempt to compare the (TC−)NBRA results to the simulation shown in Figure 3c (nor Figure 3a). Figure 3a and c are shown merely for the sake of completeness and could be used to analyze NBRA or TC-NBRA results if the initial electronic state in such calculations were initialized to be the ground state. Another observation concerning the non-NBRA results is that, for the second trajectory (Figure 3d), the population of the third state does not decay to zero completely but rather thermalizes and reaches the level of roughly 0.3. Considering the PES profile (Figure 1b), all three states are closely spaced at their minima; therefore, observing the equilibrium population of about 1/3 is reasonable.

The population dynamics computed with the standard NBRA is shown in Figure 3c and d. For each of the two guiding trajectories, a complete relaxation of initial state 3 is observed. It is faster for the guiding trajectory that started on the second excited state (Figure 3d), yielding 38 ± 9 fs, nearly identical to the result of the non-NBRA, 36 fs (Figure 3d). This is not

https://doi.org/10.1021/acs.jpclett.3c03029
J. Phys. Chem. Lett. 2023, 14, 11673−11683

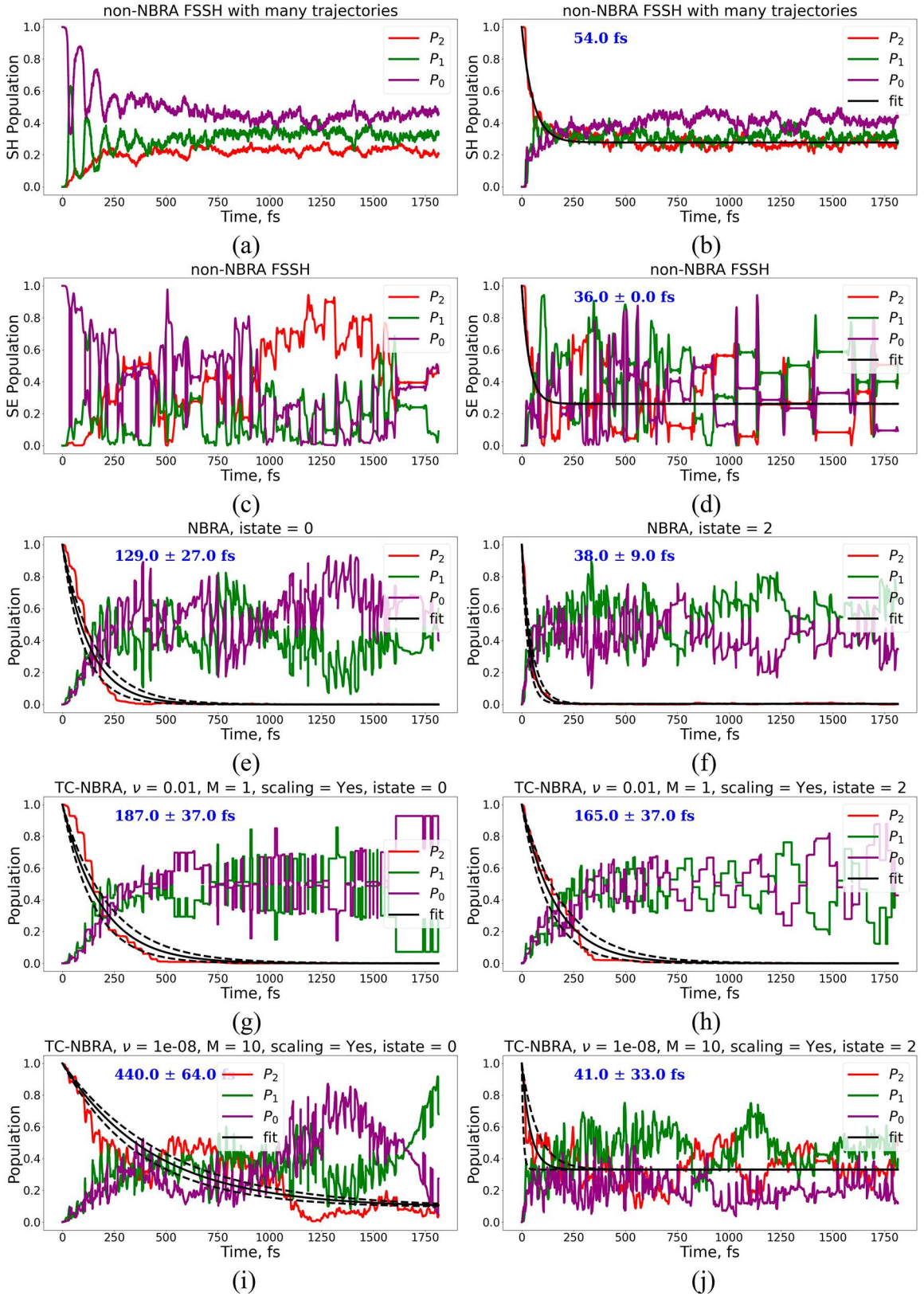

Figure 3. Comparison of the population dynamics computed with different methods. (a and b) Genuine non-NBRA FSSH calculations with multiple trajectories. (c and d) TD-SE populations, $|C_i|^2$, along the guiding trajectories obtained with "istate = 0" (panel c) or "istate = 2" (panel d) and used in the subsequent NBRA calculations. (e and f) tStandard NBRA approach with the bath temperature of T = 300 K. (g and h) TC-NBRA with a high thermostat frequency, one Nosé−Hoover thermostat particle, and NAC scaling activated. (I and j) TC-NBRA with a very low thermostat frequency, 10 Nosé−Hoover thermostat particles, and NAC scaling activated. The left column (panels a, c, e, g, and i) corresponds to the trajectories computed starting on the ground electronic state ("istate = 0"), and the right column (panels b, d, f, h, and j) corresponds to the trajectories computed starting of the second excited state ("istate = 2").

https://doi.org/10.1021/acs.jpclett.3c03029
J. Phys. Chem. Lett. 2023, 14, 11673−11683

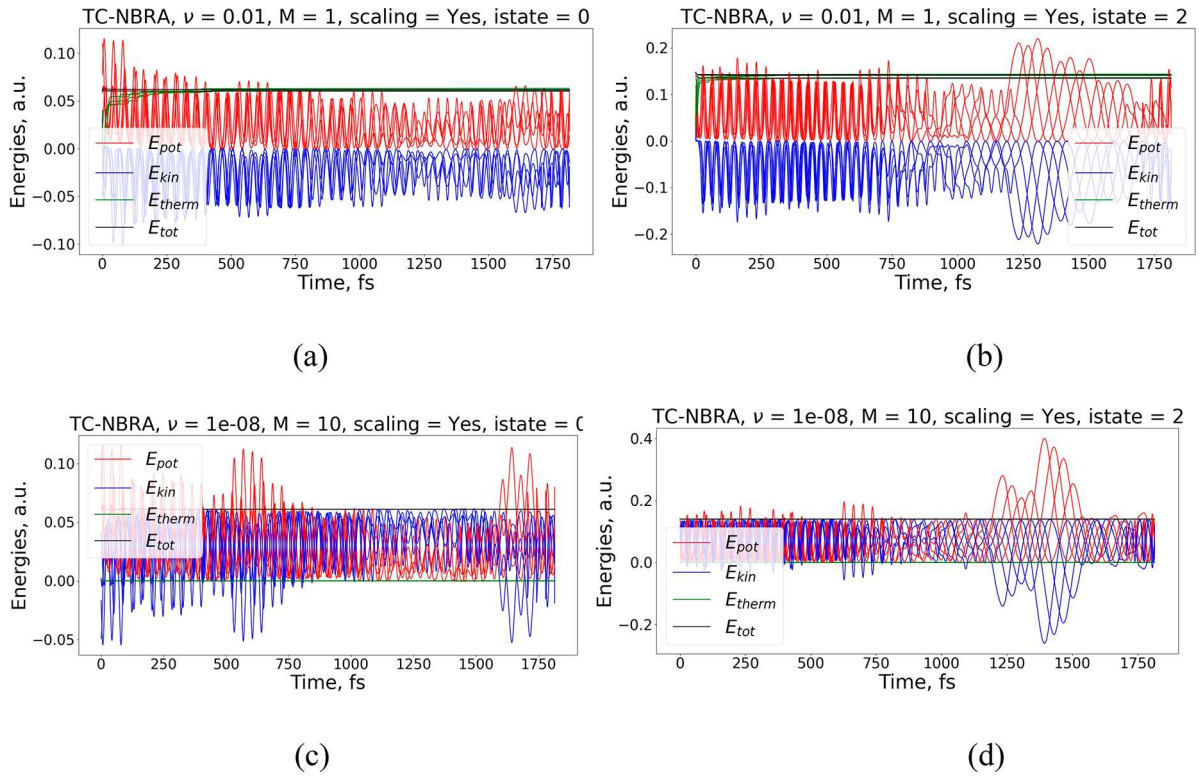

Figure 4. Energy balance in the TC-NBRA dynamics. (a and b) High thermostat frequency case (ν = 0.01 au): the energy quickly dissipates into the thermostat (green lines). (c and d) Very low frequency case ($\nu = 10^{-8}$ au): the thermostat is effectively decoupled, its energy is zero, so thermal re-excitation of the system is possible, leading to nonzero equilibrium populations of excited states. Color code: red, potential energy; blue, kinetic energy; green, thermostat energy; and black, total energy of the system plus thermostat energy. For each property, four lines appear corresponding to each batch of simulations.

surprising, since the trajectory is such that it reaches the strong NAC region at q_0 around 1−4 au by descending from $q_0 = -4$ on excited state 2 PES, E_2, (purple surface). The NBRA relaxation time computed using the ground-state guiding trajectory is larger, 129 ± 27 fs. This is because although the dynamics still reaches the strong NAC region (due to initial energy level), the slope of the ground-state surface, E_0 (red), is smaller than that of E_2, so it takes longer for the system to reach this point at which notable population transfer occurs.

The TC-NBRA calculations with a reasonable but relatively high frequency of the thermostat ν = 0.01 au lead to relaxation dynamics slower than the one obtained in the NBRA (Figure 3e and f). Similar to other situations, the dynamics for the second guiding trajectory (istate = 2) is somewhat faster than that for the other, likely for the same reasons as above. Analogously to the NBRA, the population of state 2 decays to zero. This is due to dissipation of energy into the thermostat (Figure 4a and b). Note that such dissipation occurs rather rapidly and essentially defines the population relaxation time scale.

The dependence of TC-NBRA dynamics on parameters of thermostat and the type of guiding trajectory is analyzed in Table 1 (please see Figures S1 and S2 in the Supporting Information for the plots of population dynamics and corresponding fits, as well as Figures S3 and S4 for the analysis of energy balance and conservation). As already mentioned above for two special cases, the time scales obtained using the second (istate = 2) guiding trajectory are smaller compared to those obtained using the first (istate = 0) guiding trajectory. This observation holds true for all parameters of thermostat tested.

Table 1. Relaxation Time Scales of State 3 as Computed in NBRA and TC-NBRA Simulations Using Various Thermostat Properties and Two Different Guiding Trajectories

	guiding trajectory with istate = 0		guiding trajectory with istate = 2	
	NAC scaling, yes	NAC scaling, no	NAC scaling, yes	NAC scaling, no
NBRA	129 ± 27	129 ± 27	38 ± 9	38 ± 9
TC-NBRA, ν = 0.01, M = 1	187 ± 37	156 ± 28	165 ± 37	141 ± 31
TC-NBRA, ν = 0.01, M = 10	192 ± 33	151 ± 31	170 ± 34	142 ± 37
TC-NBRA, $\nu = 10^{-4}$, M = 1	237 ± 44	166 ± 37	159 ± 47	112 ± 41
TC-NBRA, $\nu = 10^{-4}$, M = 10	251 ± 40	175 ± 39	161 ± 56	135 ± 49
TC-NBRA, $\nu = 10^{-8}$, M = 10	440 ± 64	396 ± 88	41 ± 33	42 ± 31

Another clear dependence observed is the inhibition of the population relaxation when NAC scaling is used. This effect is observed for all thermostat frequencies, all numbers of thermostat particles, and both guiding trajectories. This effect can be rationalized by quick kinetic energy damping by the thermostat. The instantaneous kinetic energy (Figure 4, panels a and c for the istate = 0 guiding trajectory and panels b and d for the istate = 2 guiding trajectory) is therefore smaller than the amount of kinetic energy in the reference calculation (which in this case was the NVE/FSSH calculation, so the reference kinetic energy is generally large, Figure 2). The maximal values

https://doi.org/10.1021/acs.jpclett.3c03029
J. Phys. Chem. Lett. 2023, 14, 11673−11683

of these quantities are comparable only in the limit of the low thermostat frequency. In other cases, the kinetic energy is quickly dissipated from the system in the TC-NBRA, so the NAC scaling tends to slow the dynamics instead of accelerating it. It is, however, possible to imagine situations when NAC scaling would lead to an acceleration of the dynamics. Indeed, consider an atomistic system in thermal equilibrium at temperature T. The reference kinetic energy would be $e_{\mathrm{kin}}^{\mathrm{ref}} = (N_f/2)k_{\mathrm{B}}T$, where N_f is the number of nuclear degrees of freedom. This energy is typically on the order of 0.001 Ha (ca. 0.025 eV) per degree of freedom. Any energy relaxation over a 0.1−1 eV range would lead to NAC amplification factors larger than 1. Thus, unless the thermostat's frequency is high enough, one can expect an acceleration of the population relaxation. Such situations can be imagined for gas-phase processes or for systems in a vacuum. In such isolated conditions, there is no energy dissipation to the environment, so the rescaling of the effective NACs would be positive (upscaling) and would accelerate the NA dynamics compared to the regular NBRA predictions.

The dependence of the relaxation time scales on the thermostat frequency is itself dependent on the choice of the guiding trajectory. For the nonequilibrium trajectory (istate = 2), the time scales are not too sensitive to the thermostat frequency, except when it is vanishing. This effect can be rationalized by the behavior expected from the thermostat in this regime. Since the system is descending from a high potential energy point down in energy, the thermostat only absorbs the excess of kinetic energy and has little chance to return kinetic energy back to system, unless its frequency is zero (in which case it does not absorb the energy). The guiding trajectory with istate = 0 is closer to the equilibrium; the generation of the kinetic energy excess is not as fast as that in the istate = 2 case. Hence, the thermostat can act bidirectionally, both by absorbing kinetic energy and by temporarily donating it back to the system, facilitating thermally induced state transitions to higher-energy states. On average, the effect of such an action is a slower relaxation of the excited state. The removal of kinetic energy is slower for thermostats with lower frequencies. Hence the period when higher energy states can be populated by thermal excitation is longer. As the overall effect, the population relaxes slower when thermostat frequency decreases (Table 1, columns 2 and 3).

The dependence on the number of thermostat particles (M) is weak; the time scales computed for $M = 1$ and $M = 10$ with all other parameters constant are within the confidence interval of each other. This is a reasonable result, since the choice of the type of thermostat is a technical parameter that should not generally affect the physics of the process, provided that the capacity of the thermostat is sufficient to absorb the kinetic energy released by the system.

Finally, in the limiting case of vanishing thermostat frequencies (Figure 3i and j), there is no energy dissipation from the system, which yields a nonzero equilibrium population for the initial state 3, making the TC-NBRA kinetics (Figure 3j) comparable to the non-NBRA dynamics (Figure 3d or even Figure 3b), both in terms of equilibrium populations and in terms of the state 3 relaxation time scale of 41 ± 33 fs (or 54 fs for multiple-trajectory non-NBRA SH population relaxation). This close agreement is observed for comparable guiding trajectories. For another guiding trajectory (Figure 3i), the state 3 relaxation time increases, yet gives some nonvanishing equilibrium population of all states rather than relaxing all excited states to zero population as in the NBRA. The relaxation time scale (440 ± 64 with NAC scaling or 396 ± 88 without) is increased compared to the NBRA value (129 ± 27); this result can be attributed to the presence of nondissipated kinetic energy in TC-NBRA, which facilitates the repopulation of excited states. As a consequence, the trajectory-averaged population of higher states decays slower than in NBRA, where thermal re-excitation is strongly inhibited by the Boltzmann factor. The energy balance for the TC-NBRA with the vanishing thermostat frequency (Figure 4c and d) shows that there is no energy transfer to the thermostat. In addition, kinetic energy is often positive and hence can promote population transfer to higher energy states. This is in contrast with the case of TC-NBRA with a frequently acting thermostat (Figure 4a and b), where the kinetic energy is often negative and hence the population transfer to upper states is prohibited.

Additionally, for infinitely slow thermostats, one can expect the TC-NBRA and non-NBRA results to be comparable to each other. Indeed, comparing Figure 3b (non-NBRA with many trajectories, SH populations) or Figure 3d (non-NBRA, 1 trajectory, SE populations) with Figure 3j (TC-NBRA with infinitely slow thermostat, many trajectories, SH populations), one can observe a close similarity of the results. In both non-NBRA and limiting TC-NBRA cases, the population of state 3 reaches a plateau at comparable populations of about 0.3. In both situations, the initial decay of the third state is observed within ca. 40 fs (a bit longer in the case of FSSH with multiple trajectories, 54 fs). However, there is still no expectation that they will be identical. The reason for such a difference of the limiting TC-NBRA case from the non-NBRA approach is that in the former the evolution of the trajectory is decoupled from the evolution of the kinetic energy variables (and hence sometimes leads to their negative value). In the non-NBRA, this does not happen.

To summarize, in this work, I present the development and assessment of the energy-conserving and thermally corrected NBRA approach for NA-MD simulations. In this new approach, an artificial thermostat is coupled to the system to control the energy dissipation rate. It is found that for strongly non-equilibrium trajectories, thermostat parameters affect the relaxation dynamics only weakly. In this regime, it is best not to use the thermostat at all, in which case the TC-NBRA results agree with the non-NBRA reference results both in producing comparable relaxation time scales and in yielding nonzero equilibrium populations of the involved states. In this regard, the TC-NBRA may be regarded as superior to the commonly used NBRA approach. For slower (closer to being equilibrium) trajectories, commonly produced in the ground state adiabatic dynamics, the thermostat has a much stronger impact on the computed relaxation time scales; lower thermostat frequencies results in slower relaxation of excited states. In this regime, the thermal correction of NACs (rescaling to account for the difference of instantaneous and reference kinetic energies) yields slower excited-state relaxation dynamics, although it is noted that such an observation may be system- and initial-condition-dependent. Similar to the case of using nonequilibrium guiding trajectories, it is also possible to achieve nonzero equilibrium populations of involved states in the limit of zero thermostat frequency (de facto decoupled thermostat). Finally, it is found that the number of thermostat particles does not generally affect the computed relaxation rates, although it is noted that such a dependence may be expected in the limit of lower thermostat capacity to absorb energy released by the system.

https://doi.org/10.1021/acs.jpclett.3c03029
J. Phys. Chem. Lett. 2023, 14, 11673−11683

■ ASSOCIATED CONTENT

Data Availability Statement

The Python scripts for all calculations and Jupyter notebook for visualization of data, as well as the archived data, are available via Zenodo (10.5281/zenodo.10208112). Libra v5.5.0 is available via Zenodo (10.5281/zenodo.10208096).

Supporting Information

The Supporting Information is available free of charge at https://pubs.acs.org/doi/10.1021/acs.jpclett.3c03029.

Population dynamics and fits for TC-NBRA and NBRA calculations and plots of the energy contributions vs time for TC-NBRA calculations (PDF)

■ AUTHOR INFORMATION

Corresponding Author

Alexey V. Akimov − *Department of Chemistry, University at Buffalo, The State University of New York, Buffalo, New York 14260, United States;* orcid.org/0000-0002-7815-3731; Email: alexeyak@buffalo.edu

Complete contact information is available at: https://pubs.acs.org/10.1021/acs.jpclett.3c03029

Notes

The author declares no competing financial interest.

■ ACKNOWLEDGMENTS

A.V.A acknowledges the financial support of the National Science Foundation (Grant NSF-2045204). Computational support is provided by the Center for Computational Research at the University at Buffalo.

■ REFERENCES

(1) Zheng, Z.; Shi, Y.; Zhou, J.-J.; Prezhdo, O. V.; Zheng, Q.; Zhao, J. Ab Initio Real-Time Quantum Dynamics of Charge Carriers in Momentum Space. *Nat. Comput. Sci.* **2023**, *3* (6), 532−541.

(2) Blumberger, J. Recent Advances in the Theory and Molecular Simulation of Biological Electron Transfer Reactions. *Chem. Rev.* **2015**, *115* (20), 11191−11238.

(3) Crespo-Otero, R.; Barbatti, M. Recent Advances and Perspectives on Nonadiabatic Mixed Quantum−Classical Dynamics. *Chem. Rev.* **2018**, *118* (15), 7026−7068.

(4) Wang, L.; Akimov, A.; Prezhdo, O. V. Recent Progress in Surface Hopping: 2011−2015. *J. Phys. Chem. Lett.* **2016**, *7* (11), 2100−2112.

(5) Akimov, A. V. Fundamentals of Trajectory-Based Methods for Nonadiabatic Dynamics. In *Comprehensive Computational Chemistry*, 1st ed.; Yáñez, M., Boyd, R. J., Eds.; Elsevier: Oxford, U.K., 2024; pp 235−272. DOI: 10.1016/B978-0-12-821978-2.00034-9.

(6) Baker, H.; Perez, C. M.; Sonnichsen, C.; Strandell, D.; Prezhdo, O. V.; Kambhampati, P. Breaking Phonon Bottlenecks through Efficient Auger Processes in Perovskite Nanocrystals. *ACS Nano* **2023**, *17* (4), 3913−3920.

(7) Jeffries, W. R.; Aikens, C. M.; Knappenberger, K. L., Jr. Symmetry-Dependent Dynamics in Au38(SC6H13)24 Revealed by Polarization-Dependent Two-Dimensional Electronic Spectroscopy. *J. Phys. Chem. C* **2023**, *127* (38), 19035−19043.

(8) Senanayake, R. D.; Akimov, A. V.; Aikens, C. M. Theoretical Investigation of Electron and Nuclear Dynamics in the [Au25(SH)-18]−1 Thiolate-Protected Gold Nanocluster. *J. Phys. Chem. C* **2017**, *121* (20), 10653−10662.

(9) Smith, B.; Akimov, A. V. Hot Electron Cooling in Silicon Nanoclusters via Landau−Zener Nonadiabatic Molecular Dynamics: Size Dependence and Role of Surface Termination. *J. Phys. Chem. Lett.* **2020**, *11* (4), 1456−1465.

(10) Smith, B.; Shakiba, M.; Akimov, A. V. Nonadiabatic Dynamics in Si and CdSe Nanoclusters: Many-Body vs Single-Particle Treatment of Excited States. *J. Chem. Theory Comput.* **2021**, *17* (2), 678−693.

(11) Shakiba, M.; Stippell, E.; Li, W.; Akimov, A. V. Nonadiabatic Molecular Dynamics with Extended Density Functional Tight-Binding: Application to Nanocrystals and Periodic Solids. *J. Chem. Theory Comput.* **2022**, *18* (9), 5157−5180.

(12) Kilina, S. V.; Kilin, D. S.; Prezhdo, O. V. Breaking the Phonon Bottleneck in PbSe and CdSe Quantum Dots: Time-Domain Density Functional Theory of Charge Carrier Relaxation. *ACS Nano* **2009**, *3* (1), 93−99.

(13) Forde, A.; Inerbaev, T.; Hobbie, E. K.; Kilin, D. S. Excited-State Dynamics of a $CsPbBr_3$ Nanocrystal Terminated with Binary Ligands: Sparse Density of States with Giant Spin−Orbit Coupling Suppresses Carrier Cooling. *J. Am. Chem. Soc.* **2019**, *141* (10), 4388−4397.

(14) Weight, B. M.; Sifain, A. E.; Gifford, B. J.; Kilin, D.; Kilina, S.; Tretiak, S. Coupling between Emissive Defects on Carbon Nanotubes: Modeling Insights. *J. Phys. Chem. Lett.* **2021**, *12* (32), 7846−7853.

(15) Kryjevski, A.; Mihaylov, D.; Kilin, D. Dynamics of Charge Transfer and Multiple Exciton Generation in the Doped Silicon Quantum Dot−Carbon Nanotube System: Density Functional Theory-Based Computation. *J. Phys. Chem. Lett.* **2018**, *9* (19), 5759−5764.

(16) Li, W.; Xue, T.; Mora-Perez, C.; Prezhdo, O. V. Ab Initio Quantum Dynamics of Plasmonic Charge Carriers. *Trends Chem.* **2023**, *5* (8), 634−645.

(17) Pradhan, E.; Magyar, R. J.; Akimov, A. V. Scaling Relationships for Nonadiabatic Energy Relaxation Times in Warm Dense Matter: Toward Understanding the Equation of State. *Phys. Chem. Chem. Phys.* **2016**, *18* (47), 32466−32476.

(18) Han, Y.; Kilin, D. Photoreactions Create Superconducting Materials. *J. Appl. Spectrosc.* **2023**, *90* (3), 639−645.

(19) Kwon, S.; Sandhu, S.; Shaik, M.; Stamm, J.; Sandhu, J.; Das, R.; Hetherington, C. V.; Levine, B. G.; Dantus, M. What Is the Mechanism of H_3^+ Formation from Cyclopropane? *J. Phys. Chem. A* **2023**, *127* (41), 8633−8638.

(20) Mai, S.; Marquetand, P.; González, L. Non-Adiabatic and Intersystem Crossing Dynamics in SO2. II. The Role of Triplet States in the Bound State Dynamics Studied by Surface-Hopping Simulations. *J. Chem. Phys.* **2014**, *140* (20), No. 204302.

(21) Usenko, S.; Schüler, M.; Azima, A.; Jakob, M.; Lazzarino, L. L.; Pavlyukh, Y.; Przystawik, A.; Drescher, M.; Laarmann, T.; Berakdar, J. Femtosecond Dynamics of Correlated Many-Body States in C60 Fullerenes. *New J. Phys.* **2016**, *18* (11), No. 113055.

(22) Liu, L.; Fang, W.-H.; Martinez, T. J. A Nitrogen Out-of-Plane (NOOP) Mechanism for Imine-Based Light-Driven Molecular Motors. *J. Am. Chem. Soc.* **2023**, *145* (12), 6888−6898.

(23) Xu, C.; Zhou, G.; Alexeev, E. M.; Cadore, A. R.; Paradisanos, I.; Ott, A. K.; Soavi, G.; Tongay, S.; Cerullo, G.; Ferrari, A. C.; Prezhdo, O. V.; Loh, Z.-H. Ultrafast Electronic Relaxation Dynamics of Atomically Thin MoS_2 Is Accelerated by Wrinkling. *ACS Nano* **2023**, *17* (17), 16682−16694.

(24) Liu, H.; Wang, A.; Zhang, P.; Ma, C.; Chen, C.; Liu, Z.; Zhang, Y.-Q.; Feng, B.; Cheng, P.; Zhao, J.; Chen, L.; Wu, K. Atomic-Scale Manipulation of Single-Polaron in a Two-Dimensional Semiconductor. *Nat. Commun.* **2023**, *14* (1), No. 3690.

(25) Yin, Y.; Zhao, X.; Ren, X.; Liu, K.; Zhao, J.; Zhang, L.; Li, S. Thickness Dependent Ultrafast Charge Transfer in BP/MoS_2 Heterostructure. *Adv. Funct. Mater.* **2022**, *32* (45), No. 2206952.

(26) Li, X.; Wang, A.; Chen, H.; Tao, W.; Chen, Z.; Zhang, C.; Li, Y.; Zhang, Y.; Shang, H.; Weng, Y.-X.; Zhao, J.; Zhu, H. Ultrafast Spontaneous Localization of a Jahn-Teller Exciton Polaron in Two-Dimensional Semiconducting CrI_3 by Symmetry Breaking. *Nano Lett.* **2022**, *22* (21), 8755−8762.

(27) Long, R.; Fang, W.; Akimov, A. V. Nonradiative Electron−Hole Recombination Rate Is Greatly Reduced by Defects in Monolayer Black Phosphorus: Ab Initio Time Domain Study. *J. Phys. Chem. Lett.* **2016**, *7* (4), 653−659.

(28) Akimov, A. V. Excited State Dynamics in Monolayer Black Phosphorus Revisited: Accounting for Many-Body Effects. *J. Chem. Phys.* **2021**, *155* (13), No. 134106.
(29) Akimov, A. V. Extending the Time Scales of Nonadiabatic Molecular Dynamics via Machine Learning in the Time Domain. *J. Phys. Chem. Lett.* **2021**, *12* (50), 12119−12128.
(30) Agrawal, S.; Lin, W.; Prezhdo, O. V.; Trivedi, D. J. Ab Initio Quantum Dynamics of Charge Carriers in Graphitic Carbon Nitride Nanosheets. *J. Chem. Phys.* **2020**, *153* (5), No. 054701.
(31) Shakiba, M.; Akimov, A. V. Dependence of Electron−Hole Recombination Rates on Charge Carrier Concentration: A Case Study of Nonadiabatic Molecular Dynamics in Graphitic Carbon Nitride Monolayers. *J. Phys. Chem. C* **2023**, *127* (19), 9083−9096.
(32) Zhu, Y.; Prezhdo, O. V.; Long, R.; Fang, W.-H. Twist Angle-Dependent Intervalley Charge Carrier Transfer and Recombination in Bilayer WS_2. *J. Am. Chem. Soc.* **2023**, *145* (41), 22826−22835.
(33) Giri, A.; Walton, S. G.; Tomko, J.; Bhatt, N.; Johnson, M. J.; Boris, D. R.; Lu, G.; Caldwell, J. D.; Prezhdo, O. V.; Hopkins, P. E. Ultrafast and Nanoscale Energy Transduction Mechanisms and Coupled Thermal Transport across Interfaces. *ACS Nano* **2023**, *17* (15), 14253−14282.
(34) Han, Y.; Iduoku, K.; Grant, G.; Rasulev, B.; Leontyev, A.; Hobbie, E. K.; Tretiak, S.; Kilina, S. V.; Kilin, D. S. Hot Carrier Dynamics at Ligated Silicon(111) Surfaces: A Computational Study. *J. Phys. Chem. Lett.* **2021**, *12* (31), 7504−7511.
(35) Vazhappilly, T.; Kilin, D. S.; Micha, D. A. Photoabsorbance of Supported Metal Clusters: Ab Initio Density Matrix and Model Studies of Large Ag Clusters on Si Surfaces. *Phys. Chem. Chem. Phys.* **2023**, *25* (21), 14757−14765.
(36) Andermann, A. M.; Rego, L. G. C. Energetics of the Charge Generation in Organic Donor−Acceptor Interfaces. *J. Chem. Phys.* **2022**, *156* (2), No. 024104.
(37) Freixas, V. M.; Oldani, N.; Tretiak, S.; Fernandez-Alberti, S. Twisting Aromaticity and Photoinduced Dynamics in Hexapole Helicenes. *J. Phys. Chem. Lett.* **2023**, *14* (45), 10145−10150.
(38) Mukazhanova, A.; Negrin-Yuvero, H.; Freixas, V. M.; Tretiak, S.; Fernandez-Alberti, S.; Sharifzadeh, S. The Impact of Stacking and Phonon Environment on Energy Transfer in Organic Chromophores: Computational Insights. *J. Mater. Chem. C* **2023**, *11* (16), 5297−5306.
(39) Alvertis, A. M.; Haber, J. B.; Engel, E. A.; Sharifzadeh, S.; Neaton, J. B. Phonon-Induced Localization of Excitons in Molecular Crystals from First Principles. *Phys. Rev. Lett.* **2023**, *130* (8), No. 086401.
(40) Ran, J.; Wang, B.; Wu, Y.; Liu, D.; Mora Perez, C.; Vasenko, A. S.; Prezhdo, O. V. Halide Vacancies Create No Charge Traps on Lead Halide Perovskite Surfaces but Can Generate Deep Traps in the Bulk. *J. Phys. Chem. Lett.* **2023**, *14* (26), 6028−6036.
(41) Zhou, Z.; He, J.; Frauenheim, T.; Prezhdo, O. V.; Wang, J. Control of Hot Carrier Cooling in Lead Halide Perovskites by Point Defects. *J. Am. Chem. Soc.* **2022**, *144* (39), 18126−18134.
(42) Smith, B.; Shakiba, M.; Akimov, A. V. Crystal Symmetry and Static Electron Correlation Greatly Accelerate Nonradiative Dynamics in Lead Halide Perovskites. *J. Phys. Chem. Lett.* **2021**, *12* (9), 2444−2453.
(43) Nijamudheen, A.; Akimov, A. V. Criticality of Symmetry in Rational Design of Chalcogenide Perovskites. *J. Phys. Chem. Lett.* **2018**, *9* (1), 248−257.
(44) Madjet, M. E.; Berdiyorov, G. R.; El-Mellouhi, F.; Alharbi, F. H.; Akimov, A. V.; Kais, S. Cation Effect on Hot Carrier Cooling in Halide Perovskite Materials. *J. Phys. Chem. Lett.* **2017**, *8* (18), 4439−4445.
(45) Duan, H.-G.; Tiwari, V.; Jha, A.; Berdiyorov, G. R.; Akimov, A.; Vendrell, O.; Nayak, P. K.; Snaith, H. J.; Thorwart, M.; Li, Z.; Madjet, M. E.; Miller, R. J. D. Photoinduced Vibrations Drive Ultrafast Structural Distortion in Lead Halide Perovskite. *J. Am. Chem. Soc.* **2020**, *142* (39), 16569−16578.
(46) Zheng, F.; Wang, L. Multiple k -Point Nonadiabatic Molecular Dynamics for Ultrafast Excitations in Periodic Systems: The Example of Photoexcited Silicon. *Phys. Rev. Lett.* **2023**, *131* (15), No. 156302.
(47) Smith, B.; Akimov, A. V. Modeling Nonadiabatic Dynamics in Condensed Matter Materials: Some Recent Advances and Applications. *J. Phys.: Condens. Matter* **2020**, *32* (7), No. 073001.
(48) Barbatti, M. Nonadiabatic Dynamics with Trajectory Surface Hopping Method. *WIREs Comput. Mol. Sci.* **2011**, *1* (4), 620−633.
(49) Zheng, Q.; Chu, W.; Zhao, C.; Zhang, L.; Guo, H.; Wang, Y.; Jiang, X.; Zhao, J. Ab Initio Nonadiabatic Molecular Dynamics Investigations on the Excited Carriers in Condensed Matter Systems. *WIREs Comput. Mol. Sci.* **2019**, *9* (6), No. e1411.
(50) Shakiba, M.; Akimov, A. V. Generalization of the Local Diabatization Approach for Propagating Electronic Degrees of Freedom in Nonadiabatic Dynamics. *Theor. Chem. Acc.* **2023**, *142* (8), No. 68.
(51) Mai, S.; Marquetand, P.; González, L. Nonadiabatic Dynamics: The SHARC Approach. *WIREs Comput. Mol. Sci.* **2018**, *8* (6), No. e1370.
(52) Tully, J. C. Molecular Dynamics with Electronic Transitions. *J. Chem. Phys.* **1990**, *93* (2), 1061−1071.
(53) Nelson, T.; Fernandez-Alberti, S.; Roitberg, A. E.; Tretiak, S. Nonadiabatic Excited-State Molecular Dynamics: Treatment of Electronic Decoherence. *J. Chem. Phys.* **2013**, *138* (22), No. 224111.
(54) Jaeger, H. M.; Fischer, S.; Prezhdo, O. V. Decoherence-Induced Surface Hopping. *J. Chem. Phys.* **2012**, *137* (22), No. 22A545.
(55) Bedard-Hearn, M. J.; Larsen, R. E.; Schwartz, B. J. Mean-Field Dynamics with Stochastic Decoherence (MF-SD): A New Algorithm for Nonadiabatic Mixed Quantum/Classical Molecular-Dynamics Simulations with Nuclear-Induced Decoherence. *J. Chem. Phys.* **2005**, *123* (23), No. 234106.
(56) Esch, M. P.; Levine, B. G. An Accurate, Non-Empirical Method for Incorporating Decoherence into Ehrenfest Dynamics. *J. Chem. Phys.* **2021**, *155* (21), No. 214101.
(57) Esch, M. P.; Levine, B. G. Decoherence-Corrected Ehrenfest Molecular Dynamics on Many Electronic States. *J. Chem. Phys.* **2020**, *153* (11), No. 114104.
(58) Esch, M. P.; Levine, B. G. State-Pairwise Decoherence Times for Nonadiabatic Dynamics on More than Two Electronic States. *J. Chem. Phys.* **2020**, *152* (23), No. 234105.
(59) Granucci, G.; Persico, M.; Zoccante, A. Including Quantum Decoherence in Surface Hopping. *J. Chem. Phys.* **2010**, *133* (13), No. 134111.
(60) Guo, X.; Xu, J.; Li, G.; Wang, L. Interpretation of Adiabatic and Diabatic Populations from Trajectories of Branching Corrected Surface Hopping. *Chin. J. Chem. Phys.* **2022**, *35*, 488.
(61) Xu, J.; Wang, L. Branching Corrected Surface Hopping: Resetting Wavefunction Coefficients Based on Judgement of Wave Packet Reflection. *J. Chem. Phys.* **2019**, *150* (16), No. 164101.
(62) Xu, J.; Wang, L. Branching Corrected Mean Field Method for Nonadiabatic Dynamics. *J. Phys. Chem. Lett.* **2020**, *11* (19), 8283−8291.
(63) Shao, C.; Xu, J.; Wang, L. Branching and Phase Corrected Surface Hopping: A Benchmark of Nonadiabatic Dynamics in Multilevel Systems. *J. Chem. Phys.* **2021**, *154* (23), No. 234109.
(64) Li, G.; Shao, C.; Xu, J.; Wang, L. A Unified Framework of Mixed Quantum−Classical Dynamics with Trajectory Branching. *J. Chem. Phys.* **2022**, *157* (21), No. 214102.
(65) Subotnik, J. E.; Shenvi, N. A New Approach to Decoherence and Momentum Rescaling in the Surface Hopping Algorithm. *J. Chem. Phys.* **2011**, *134* (2), No. 024105.
(66) Jain, A.; Alguire, E.; Subotnik, J. E. An Efficient, Augmented Surface Hopping Algorithm That Includes Decoherence for Use in Large-Scale Simulations. *J. Chem. Theory Comput.* **2016**, *12* (11), 5256−5268.
(67) Landry, B. R.; Subotnik, J. E. Communication: Standard Surface Hopping Predicts Incorrect Scaling for Marcus' Golden-Rule Rate: The Decoherence Problem Cannot Be Ignored. *J. Chem. Phys.* **2011**, *135* (19), No. 191101.
(68) Miao, G.; Subotnik, J. Revisiting the Recoherence Problem in the Fewest Switches Surface Hopping Algorithm. *J. Phys. Chem. A* **2019**, *123* (26), 5428−5435.

https://doi.org/10.1021/acs.jpclett.3c03029
J. Phys. Chem. Lett. 2023, 14, 11673−11683

(69) Shenvi, N.; Subotnik, J. E.; Yang, W. Phase-Corrected Surface Hopping: Correcting the Phase Evolution of the Electronic Wavefunction. *J. Chem. Phys.* **2011**, *135* (2), No. 024101.
(70) Plasser, F.; Granucci, G.; Pittner, J.; Barbatti, M.; Persico, M.; Lischka, H. Surface Hopping Dynamics Using a Locally Diabatic Formalism: Charge Transfer in the Ethylene Dimer Cation and Excited State Dynamics in the 2-Pyridone Dimer. *J. Chem. Phys.* **2012**, *137* (22), No. 22A514.
(71) Akimov, A. V. A Simple Phase Correction Makes a Big Difference in Nonadiabatic Molecular Dynamics. *J. Phys. Chem. Lett.* **2018**, *9* (20), 6096−6102.
(72) Zhou, Z.; Jin, Z.; Qiu, T.; Rappe, A. M.; Subotnik, J. E. A Robust and Unified Solution for Choosing the Phases of Adiabatic States as a Function of Geometry: Extending Parallel Transport Concepts to the Cases of Trivial and Near-Trivial Crossings. *J. Chem. Theory Comput.* **2020**, *16* (2), 835−846.
(73) Meek, G. A.; Levine, B. G. Evaluation of the Time-Derivative Coupling for Accurate Electronic State Transition Probabilities from Numerical Simulations. *J. Phys. Chem. Lett.* **2014**, *5* (13), 2351−2356.
(74) Craig, C. F.; Duncan, W. R.; Prezhdo, O. V. Trajectory Surface Hopping in the Time-Dependent Kohn-Sham Approach for Electron-Nuclear Dynamics. *Phys. Rev. Lett.* **2005**, *95* (16), No. 163001.
(75) Duncan, W. R.; Prezhdo, O. V. Theoretical Studies of Photoinduced Electron Transfer in Dye-Sensitized TiO_2. *Annu. Rev. Phys. Chem.* **2007**, *58* (1), 143−184.
(76) Prezhdo, O. V.; Duncan, W. R.; Prezhdo, V. V. Photoinduced Electron Dynamics at the Chromophore−Semiconductor Interface: A Time-Domain Ab Initio Perspective. *Prog. Surf. Sci.* **2009**, *84* (1−2), 30−68.
(77) Wang, Z.; Dong, J.; Qiu, J.; Wang, L. All-Atom Nonadiabatic Dynamics Simulation of Hybrid Graphene Nanoribbons Based on Wannier Analysis and Machine Learning. *ACS Appl. Mater. Interfaces* **2022**, *14* (20), 22929−22940.
(78) Oliboni, R. S.; Yan, H.; Fan, H.; Abraham, B.; Avenoso, J. P.; Galoppini, E.; Batista, V. S.; Gundlach, L.; Rego, L. G. C. Vibronic Effects in the Ultrafast Interfacial Electron Transfer of Perylene-Sensitized TiO_2 Surfaces. *J. Phys. Chem. C* **2019**, *123* (20), 12599−12607.
(79) Giannini, S.; Di Virgilio, L.; Bardini, M.; Hausch, J.; Geuchies, J. J.; Zheng, W.; Volpi, M.; Elsner, J.; Broch, K.; Geerts, Y. H.; Schreiber, F.; Schweicher, G.; Wang, H. I.; Blumberger, J.; Bonn, M.; Beljonne, D. Transiently Delocalized States Enhance Hole Mobility in Organic Molecular Semiconductors. *Nat. Mater.* **2023**, *22* (11), 1361−1369.
(80) Peng, W.-T.; Brey, D.; Giannini, S.; Dell'Angelo, D.; Burghardt, I.; Blumberger, J. Exciton Dissociation in a Model Organic Interface: Excitonic State-Based Surface Hopping versus Multiconfigurational Time-Dependent Hartree. *J. Phys. Chem. Lett.* **2022**, *13* (31), 7105−7112.
(81) Malone, W.; Nebgen, B.; White, A.; Zhang, Y.; Song, H.; Bjorgaard, J. A.; Sifain, A. E.; Rodriguez-Hernandez, B.; Freixas, V. M.; Fernandez-Alberti, S.; Roitberg, A. E.; Nelson, T. R.; Tretiak, S. NEXMD Software Package for Nonadiabatic Excited State Molecular Dynamics Simulations. *J. Chem. Theory Comput.* **2020**, *16* (9), 5771−5783.
(82) Freixas, V. M.; Malone, W.; Li, X.; Song, H.; Negrin-Yuvero, H.; Pérez-Castillo, R.; White, A.; Gibson, T. R.; Makhov, D. V.; Shalashilin, D. V.; Zhang, Y.; Fedik, N.; Kulichenko, M.; Messerly, R.; Mohanam, L. N.; Sharifzadeh, S.; Bastida, A.; Mukamel, S.; Fernandez-Alberti, S.; Tretiak, S. NEXMD v2.0 Software Package for Nonadiabatic Excited State Molecular Dynamics Simulations. *J. Chem. Theory Comput.* **2023**, *19* (16), 5356−5368.
(83) Mejia-Rodriguez, D.; Aprà, E.; Autschbach, J.; Bauman, N. P.; Bylaska, E. J.; Govind, N.; Hammond, J. R.; Kowalski, K.; Kunitsa, A.; Panyala, A.; Peng, B.; Rehr, J. J.; Song, H.; Tretiak, S.; Valiev, M.; Vila, F. D. NWChem: Recent and Ongoing Developments. *J. Chem. Theory Comput.* **2023**, *19* (20), 7077−7096.
(84) Akimov, A. V. Libra: An Open-Source "Methodology Discovery" Library for Quantum and Classical Dynamics Simulations. *J. Comput. Chem.* **2016**, *37* (17), 1626−1649.
(85) Shakiba, M.; Smith, B.; Li, W.; Dutra, M.; Jain, A.; Sun, X.; Garashchuk, S.; Akimov, A. Libra: A Modular Software Library for Quantum Nonadiabatic Dynamics. *Softw. Impacts* **2022**, *14*, 100445.
(86) Kamberaj, H.; Low, R. J.; Neal, M. P. Time Reversible and Symplectic Integrators for Molecular Dynamics Simulations of Rigid Molecules. *J. Chem. Phys.* **2005**, *122* (22), No. 224114.
(87) Barbatti, M. Velocity Adjustment in Surface Hopping: Ethylene as a Case Study of the Maximum Error Caused by Direction Choice. *J. Chem. Theory Comput.* **2021**, *17* (5), 3010−3018.
(88) Parandekar, P. V.; Tully, J. C. Mixed Quantum-Classical Equilibrium. *J. Chem. Phys.* **2005**, *122* (9), No. 094102.
(89) Parandekar, P. V.; Tully, J. C. Detailed Balance in Ehrenfest Mixed Quantum-Classical Dynamics. *J. Chem. Theory Comput.* **2006**, *2* (2), 229−235.
(90) Schmidt, J. R.; Parandekar, P. V.; Tully, J. C. Mixed Quantum-Classical Equilibrium: Surface Hopping. *J. Chem. Phys.* **2008**, *129* (4), No. 044104.

https://doi.org/10.1021/acs.jpclett.3c03029
J. Phys. Chem. Lett. 2023, 14, 11673−11683